Earthquake hazard characterization by using entropy: application to northern Chilean earthquakes

Antonio Posadas[1, 2], Denisse Pasten [3], Eugenio E. Vogel [4,5], Gonzalo Saravia[6]

[1]Departamento de Química y Física, Universidad de Almeria, 04120 Almeria, Spain.
[2]Instituto Andaluz de Geofísica, Campus Universitario de Cartuja, Universidad de Granada, 18071 Granada, Spain
[3]Departamento de Física, Facultad de Ciencias, Universidad de Chile, Santiago, Chile
[4]Departamento de Ciencias Físicas, Universidad de La Frontera, Casilla 54-D, Temuco, Chile
[5]Center for Nanoscience and Nanotechnology (CEDENNA), Santiago, Chile
[6]Los Eucaliptus 1189, Temuco 4812537, Chile

Correspondence to: Antonio Posadas (aposadas@ual.es)

Abstract. The mechanical description of the seismic cycle has an energetic analogy in terms of statistical physics and the Second Law of Thermodynamics. In this context, an earthquake can be considered as a phase transition, where continuous reorganization of stresses and forces reflects an evolution from equilibrium to non-equilibrium states and we can use this analogy to characterize the earthquake hazard of a region. In this study, we used 8 years (2007–2014) of high-quality Integrated Plate Boundary Observatory Chile (IPOC) seismic data for >100,000 earthquakes in northern Chile to test the theory that Shannon entropy, *H*, is an indicator of the equilibrium state of a seismically active region. We confirmed increasing *H* reflects the irreversible transition of a system and is linked to the occurrence of large earthquakes. Using variation in *H*, we could detect major earthquakes and their foreshocks and aftershocks, including 2007 M_W 7.8 Tocopilla earthquake, 2014 M_W 8.1 Iquique earthquake, and the 2010 and 2011 Calama earthquakes (M_W 6.6 and 6.8, respectively). Moreover, we identified possible periodic seismic behaviour between 80 and 160 km depth.

1 Introduction

The seismicity of a region contains abundant information that can be used, from different points of view, attempting to know when an earthquake is going to occur. In physics, Entropy is one of the most fascinating, abstract and complex concepts. The present paper shows how to use Entropy to characterize the occurrence of earthquakes, i.e. to have a characterisation of the seismic hazard in entropic terms.

It is well known (e.g. Nikulov, 2022) that the second law of thermodynamics postulates the existence of irreversible processes in physics: the total entropy of an isolated system can increase, but cannot decrease. Namely, only those phenomena for which the entropy of the universe increases are allowed. Thus, in seismology, it is natural to use entropy to find out future states that a region of the Earth's crust can access from its current state (Akopian, 2015).

The concept of entropy and its connection to the Second Law of Thermodynamics was proposed by Clausius in 1865 (Clausius, 1865) and a few years later, Boltzmann realised that entropy could be used to connect the microscopic motion of particles to the macroscopic world; in his analysis, entropy (S) is proportional to the number of accessible micro-states of the system (Ω) and is expressed by the famous Boltzmann equation:

$$S = k \ln \Omega \,, \tag{1}$$

where k is Boltzmann's constant. Ben-Naim (2020) stated that, at first glance, Boltzmann's entropy and Clausius' entropy are absolutely different; however, there is complete agreement in calculating changes in entropy using the two methods (up to a multiplicative constant). The generalization of Boltzmann's entropy for systems described by other macroscopic variables corresponded to Gibbs (Zupanovic and Domagoj, 2018) and can be written as:

$$S = -k \sum_{i=1}^{\Omega} p_i \log\, p_i \,, \tag{2}$$

where p_i is the probability of the system being in the *i-th* state. Shannon (1948) and Shannon and Weaver (1949) introduced Boltzmann-Gibbs's entropy concept into communication theory and defined the measure of information as:

$$I(p) = \sum_{i=1}^{\Omega} p_i \log\, p_i \,, \tag{3}$$

where p is the distribution of states and p_i is the relative frequency for each event i. The function $I(p)$ is called 'Shannon information' because it is a measure of knowledge; therefore, $-I(p)$ denotes a lack of knowledge or ignorance as Majewski (2001) has highlighted. Clearly, $I(p)$ is always negative or zero; as such, it is possible to define the 'Shannon information entropy' (*H*) as the negative information measure (Ben-Naim, 2017); that is:

$$H(p) = -I(p) = -\sum_{i=1}^{\Omega} p_i \log\, p_i \,, \tag{4}$$

which is always positive or zero. In the last equation it has been assumed, for simplicity (Truffet, 2018), that k = 1, or equivalently, that $H(p) = -{}^{I(p)}/_{k}$. Some (relatively) recent research carried out in the field of information theory suggests that the above expressions can be generalised. Thus, Tsallis (1988) proposed the use of:

$$S_\tau = \frac{k}{\tau - 1}\left(1 - \sum_{i=1}^{\Omega} p_i^\tau\right) \,, \tag{5}$$

where τ is called the entropic index and can, in principle, be any real number. The standard distribution that characterises Boltzmann-Gibbs statistics is a particular case of Tsallis entropy in the limit of τ = 1. Others generalizations, such as Renyi entropy, can be found in the scientific literature (e.g. Majewski and Teisseyre, 1997).

From the point of view of classical thermodynamics (Varotsos *et al.*, 2011; Vargas *et al.*, 2015; Sarlis *et al.*, 2018; Vogel *et al.*, 2020; Telesca *et al.*, 2022, Varotsos *et al.*, 2022), but also statistical mechanics (Michas *et al.*, 2013; Vallianatos *et al.*, 2015; Papadakis *et al.*, 2015; Vallianatos *et al.*, 2016; Vallianatos *et al.*, 2018), variation in Entropy has been widely used in seismology as an indicator of the evolution of a system (from precursor papers such as Rundle *et al.*, 2003 or Sornette and Werner, 2009, to recent ones from Posadas *et al.*, 2021, Pasten *et al.*, 2022 or Posadas and Sotolongo, 2023).

In this paper, we used 8 years (2007–2014) of high-quality Integrated Plate Boundary Observatory Chile (IPOC) seismic data for >100,000 earthquakes in northern Chile to test the theory that Shannon entropy, *H*, is an indicator of the equilibrium state of a seismically active region. Moreover, we will rough out a thermodynamics vision of the seismic cycle to characterize the seismic hazard of the northern Chilean seismicity.

2 Methods

2.1 Theoretical framework

Let us start with a representation of the state of a given seismically active region from the distribution of earthquakes with magnitudes *M* associated with time *t*; that is, $P(M)$. Thus, entropy, *H*, postulated by Shannon, which is associated with information flow, can be reformulated (De Santis *et al.*, 2019) as:

$$H\,(t) = -\int_{M_0}^{M_{max}} P(M) \cdot log(P(M))dM \tag{6}$$

where M_0 is the threshold magnitude (i.e., the magnitude for which the seismic catalogue is complete) and M_{max} is the maximum magnitude up to which earthquakes occur. There are two restrictive conditions to solve that integral. First:

$$\int_{M_0}^{M_{max}} P(M)dM = 1 \tag{7}$$

The second arises from the fact that the average value of all possible magnitudes $\bar{M}$, in a certain period, is:

$$\bar{M} = \int_{M_0}^{M_{max}} M \cdot P(M)dM \tag{8}$$

The Second Law of Thermodynamics requires that there exists a distribution under which *H* would be at its maximum value while under the two restrictive conditions; that is, the spontaneous development of the system from a state of non-equilibrium to a state of equilibrium is a process in which entropy increases and the final state of equilibrium corresponds to the maximum entropy. Thus, the problem can be solved by applying the Lagrange multiplier method; to do that, we define the lagrangian $\mathcal{L}$ as:

$$\mathcal{L}\left(P(M)\right) = H(P(M)) - \lambda_1 \int_{M_0}^{M_{max}} P(M)dM - \lambda_2 \int_{M_0}^{M_{max}} M\,P(M)\,dM \tag{9}$$

where λ_1 and λ_2 are Lagrange's multipliers; then, it is possible to deduce the probability density function in the form (Feng and Luo, 2009):

$$P(M) = \frac{1}{\bar{M} - M_0}\exp\left(-\frac{M - M_0}{\bar{M} - M_0}\right) \tag{10}$$

On the other hand, if we have *N* earthquakes and *n* denotes the number of earthquakes with magnitude equal to or larger than M:

$$P(M) = \frac{n}{N} \tag{11}$$

then, we match both formulas and take logarithms to get:

$$\log n = \log\left(\frac{N}{\bar{M} - M_0}\right) + \frac{M_0 \cdot \log(e)}{\bar{M} - M_0} - \frac{\log(e)}{\bar{M} - M_0} \cdot M \tag{12}$$

But, the Gutenberg-Richter relationship (Gutenberg and Richter, 1944) states that the distribution of earthquake magnitudes follows an empirical and universal relationship:

$$\log\, n = a - bM \tag{13}$$

where n is the cumulative number of earthquakes with a magnitude equal to or larger than *M*, and *a* and *b* are real constants that may vary in space and time. Parameter *a* characterises the general level of seismicity in a given area during the study period (i.e., the higher the *a* value, the higher the seismicity), whereas parameter *b*, which is typically close to 1, describes the relative abundance of large to smaller shocks. Now, identifying terms from Eqs. 12 and 13, we obtain:

$$a = log\left(\frac{N}{\bar{M} - M_0}\right) + \frac{M_0 \cdot log(e)}{\bar{M} - M_0} \quad (14)$$

and

$$b = \frac{\log(e)}{\bar{M} - M_0} \quad (15)$$

Hence, the probability density function (Eq. 10) can be rewritten as:

$$P(M) = \frac{b}{\log(e)} \cdot 10^{-b(M - M_0)} \quad (16)$$

and, finally, substituting into Eq. 6, we get (De Santis *et al.*, 2011):

$$H = -\int_{M_0}^{\infty} \frac{b \cdot 10^{-b(M - M_0)}}{\log(e)} \cdot \log\left(\frac{b \cdot 10^{-b(M - M_0)}}{log(e)}\right) dM =$$

$$= -\log(b) + \log(e \cdot log(e)) \quad (17)$$

After computing b from the classical Utsu expression (Utsu, 1965):

$$b = \frac{\log(e)}{\bar{M} - (M_0 - \frac{\Delta M}{2})} \quad (18)$$

where ΔM is the resolution of magnitude (usually $\Delta M = 0.1$), the value of entropy can be found.

2.2 Methodology

Our analysis approach included three steps:

1. First, the value of the threshold magnitude (M_0) is a critical choice. There are two main classes of methods to evaluate M_0: catalogue-based methods (e.g., Amorèse, 2007) and network-based methods (e.g., D'Alessandro *et al.*, 2011). We used a catalogue-based method because the necessary inputs were available from our dataset. Although some studies estimate the value of M_0 by fitting the linear Gutenberg–Richter relationship to the observed frequency–magnitude distribution (the magnitude at which the lower end of the frequency–magnitude distribution departs from the Gutenberg–Richter relationship is taken as M_0 (Zúñiga and Wyss, 1995)), several other methods can better determine the threshold magnitude. Catalogue-based techniques include day-to-night noise modulation

(day/night method) (Rydele and Sacks, 1989), the Entire Magnitude Range (Ogata and Katsura, 1993), the MAXC technique or Goodness-of-Fit Test (GFT) (Wiemer and Wyss, 2000), b-value stability (MBS) (Cao and Gao, 2002), and median-based analysis of the segment slope (MBASS) (Amorèse, 2007). The MAXC technique is mainly used in applied techniques and was chosen here; however, the results do not differ significantly among these approaches.

2. Second, the time interval W was determined for the calculation of entropy (equation 17), using the minimum number of earthquakes to calculate H. The time interval can be chosen by defining a cumulative, moving, or overlapping earthquake window. Here, the results are presented for a sliding window to avoid the memory effect. It turns out that the results are substantially the same regardless of the approach taken. On the whole, the final window size offered a reasonable compromise between resolution and smoothing. The width of the window was chosen by following the approach of De Santis *et al.* (2011), which is based on meaningful values of b. In short, 200 events is the minimum needed to perform a robust statistical estimation of b and H. This has been confirmed by previous statistical analyses of a and b values (Utsu, 1999). However, larger values of W can be adopted depending on the relative error when entropy is computed (Posadas *et al.*, 2021); this criterion is explained below in the Results section.

3. Finally, the entropy function was obtained for each time t following Eq. 17. By convention, the time attributed to each point of the analyses was the time of the last seismic event considered in each window. The occurrence of a large earthquake (or the accumulation of several important ones) is expected to lead the seismic system to a state of greater disorder. Then, any earthquake is an irreversible transition to a new state carrying an increase in entropy. Once the major shock is over, entropy returns to stable values.

3 Data: the northern Chilean seismicity

The Pacific Ring of Fire, a 40,000 km horseshoe marking the tectonic boundaries of the Pacific Ocean (primarily along the boundaries of the Pacific Plate), hosts 90% of Earth's seismic activity and 75% of the active volcanoes. Also known as the Circum-Pacific Belt, it extends from Tonga and the New Hebrides islands through Indonesia, the Philippines, Japan, the Kuril and the Aleutian Islands, to the western coast of North America, before ending in the Cordillera de los Andes of South America. Among these regions, the Northern Chile Forearc experiences abundant interplate and intraplate earthquakes, intermediate and deep earthquakes associated with subduction, and a high tsunami risk along coastal areas. Events such as 2007 M_W 7.8 Tocopilla earthquake (Delouis *et al.*, 2009), 2010 M_W 8.8 Maule megathrust earthquake (Derode *et al.*, 2021), and 2014 M_W 8.1 Iquique earthquake (Cesca *et al.*, 2016) highlight the special relevance of this region. As such, monitoring seismic and volcanic activity in northern Chile using dense seismic networks (permanent and temporary) to create extensive high-quality seismic

catalogues is a priority. To this end, the Integrated Plate Boundary Observatory Chile (IPOC), established by a network of European and South American institutions, operates a wide system of instruments and projects dedicated to the study of earthquakes and deformation at the continental margin of Chile (https://www.ipoc-network.org/). The network extends from the Peru–Chile border in the north to the city of Antofagasta in the south, and from the coast in the west to the high Andes in the east.

Table 1. Earthquakes with magnitudes of > 6.5 in the Integrated Plate Boundary Observatory Chile (IPOC) catalogue for the period 2007 to 2014.

Date (yyyy/mm/dd)	Time	Latitude	Longitude	Depth (km)	M_W	Name
2007/11/14	15:40:50	−22,332	−70,044	49.24	7.8	Tocopilla earthquake
2007/12/16	08:09:13	−23,298	−70,379	64.22	6.9	Aftershock of Tocopilla earthquake
2010/03/04	22:39:24	−22,391	−68,572	109.51	6.6	Calama 2010 earthquake
2011/06/20	16:35:58	−21,894	−68,554	132.84	6.8	Calama 2011 earthquake
2014/03/16	21:16:28	−19,955	−70,860	17.86	6.6	Foreshock of Iquique earthquake
2014/04/01	23:46:46	−19,589	−70,940	19.91	8.1	Iquique earthquake
2014/04/03	02:43:14	−20,595	−70,585	21.96	7.6	Aftershock of Iquique earthquake

In this study, we used high-quality IPOC data from 2007 to 2014 (the period for which data are publicly available) to test the theory that Shannon entropy (we will use Shannon entropy but whatever other such as Tsallis entropy, e.g. Vallianatos *et al.*, 2015, Vallianatos *et al.*, 2018, Khordad *et al.*, 2022 or Rastegar *et al.*, 2022 could be adopted) represents an indicator of the equilibrium state of a seismically active region (or seismic system); we hypothesized that the relationship between increasing entropy and the occurrence of large earthquakes reflects the irreversible transition of a system. The data included records of 101,601 accurately located earthquakes within an epicentral area of 17ºS–25ºS and 66ºW–72ºW (Figure 1a). A comprehensive study of the dataset can be found in Sippl *et al.* (2018).

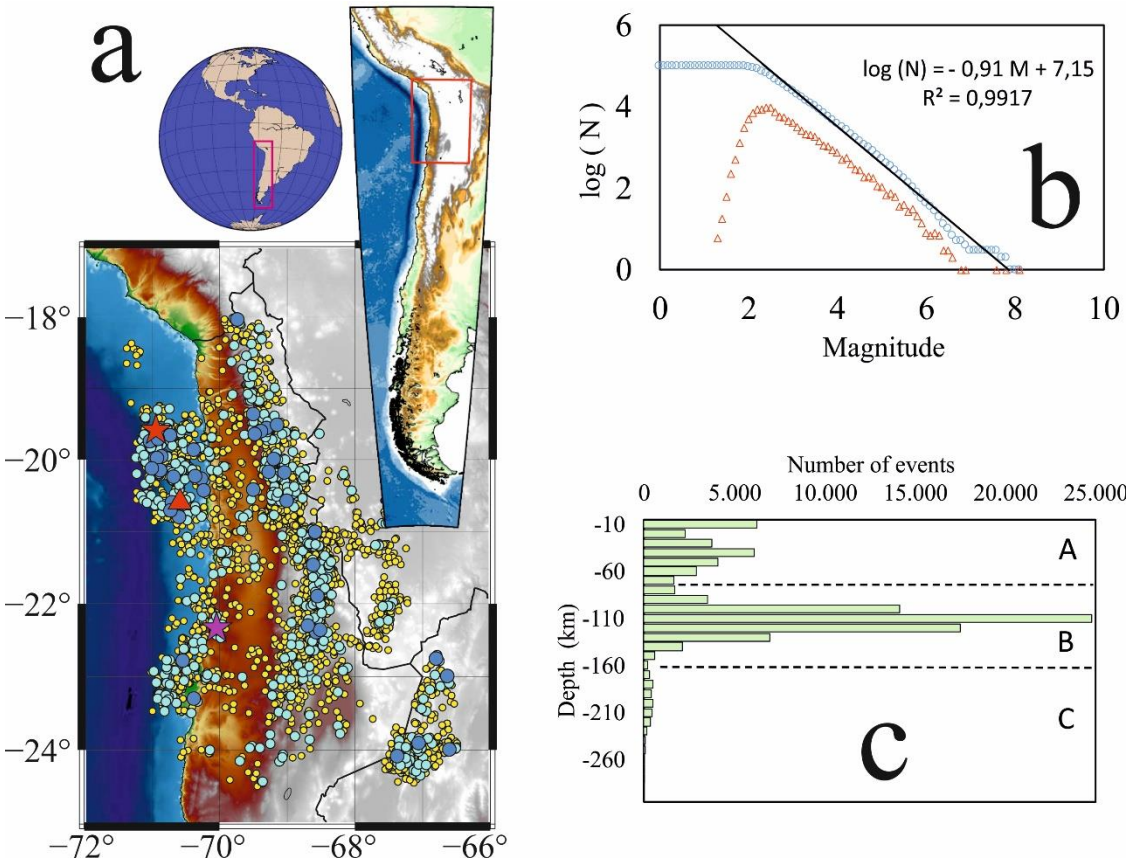

Figure 1. (a) Seismicity within an epicentral area of 17ºS–25ºS and 66ºW–72ºW between 2007 and 2014. Data are from the Integrated Plate Boundary Observatory Chile (IPOC) catalogue, which contains > 100,000 earthquakes; however, only events with magnitudes of > 4.0 are shown here (3,960 events in total). Circle colours denote event magnitudes: yellow = 4.0–4.9, cyan = 5.0–5.9, and blue = 6.0–6.9. Earthquakes with magnitudes of > 7.0 include 2007 M_W 7.8 Tocopilla earthquake (magenta star), 2014 M_W 8.1 Iquique earthquake (red star), and its main aftershock (M_W = 7.6, shown by the red triangle). (b) Gutenberg–Richter relationship. Blue circles denote the cumulative number of earthquakes; red triangles denote the non-cumulative number of earthquakes. Based on the maximum curvature (MAXC) technique (Wiemer and Wyss, 2000), $M_0 = 2.2$. (c) Histogram of earthquake depth. Bins have a 10 km resolution and three regions can be differentiated: zone A (up to 80 km depth), zone B (80–160 km depth), and zone C (> 160 km depth).

190

4 Results

Earthquakes included in the catalog have depths ranging from 0 to 300 km; It is evident that the seismic behavior of the shallower part is different from that of the deeper zone and so they should be analyzed separately. However, first, we begin with a preliminary
195 analysis of the whole catalog to show whether the used technique could recognize earthquakes of greater magnitude. Subsequently, in a more detailed approach, a second analysis will be carried out that takes into account the depths (and, therefore, the different physical behaviors associated with seismicity in each region).

The seismic catalogue contains 32 earthquakes with magnitudes of 6.0 or greater, 7 of which have magnitudes of > 6.5 (Table 1). The two largest earthquakes are the M_W 7.8 Tocopilla earthquake (November 14, 2007) and M_W 8.1 Iquique earthquake (April 1, 2014). Figure 2 shows a time series of events for earthquakes with magnitudes of > 4.0; the number of earthquakes versus time is shown in Figure 3.

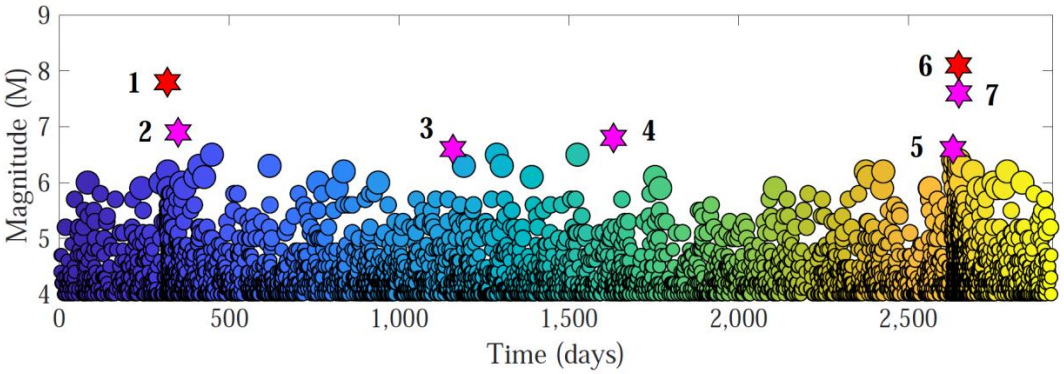

Figure 2. Magnitude versus time for earthquakes with magnitudes of > 4.0 within an epicentral area of 17ºS–25ºS and 66ºW–72ºW. Stars correspond to the earthquakes listed in Table 1, including the (1) 2007 M_W 7.8 Tocopilla earthquake, (2) 2007 M_W 6.9 Tocopilla aftershock, (3) 2010 M_W 6.6 Calama earthquake, (4) 2011 M_W 6.8 Calama earthquake, (5) M_W 6.6 foreshock of the Iquique earthquake, (6) M_W 8.1 Iquique earthquake, and (7) M_W 7.6 aftershock of the Iquique earthquake. Circles' size increases gradually with magnitude and colour, from blue to yellow, highlighting the temporal evolution.

.

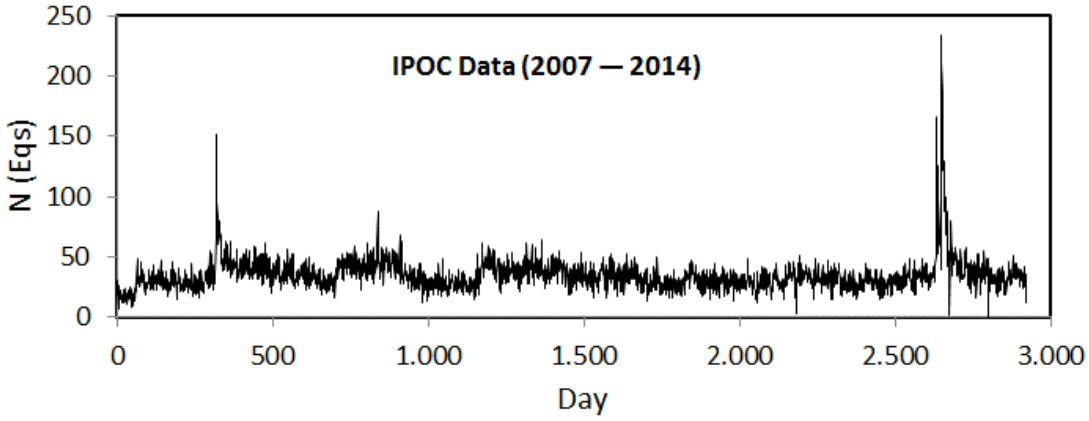

Figure 3. Number of daily earthquakes from 2007 to 2014 within an epicentral area of 17ºS–25ºS and 66ºW–72ºW. The seismic crises associated with the 2007 M_w 7.8 Tocopilla earthquake and 2014 M_w 8.1 Iquique earthquakes are clearly distinguished by the two prominent peaks.

First, the threshold magnitude M_0 is needed; to get it, we used the MAXC technique as we have mentioned before. Then, the Gutenberg-Richter relationship was got (Figure 1b) and a value of $M_0 = 2.2$ is found.

The second step of our method is to determine the width of window *W* for the windowing process. Figure 4 shows the relative error of entropy versus window width. The choice of *W* must consider that values of *b* should be significant. One way to objectify this choice of *W* is to study the relative error when obtaining the entropy. Utsu's formalism (Utsu 1965) showed that the uncertainty associated with *b* value, interpreted as the error in the *b* value determination, is given by:

$$\sigma = \frac{b}{\sqrt{N}} \tag{19}$$

From the expressions 17 and 19, it is easy to get that, for an entropy value *H*, the error margins are:

$$\Delta H = \log\left(\frac{b + \Delta b}{b - \Delta b}\right) \tag{20}$$

Hence, the relative error can be calculated as:

$$\varepsilon\,(\%) = \frac{100}{H} \cdot log\left(\frac{b + \Delta b}{b - \Delta b}\right) \tag{21}$$

From Figure 4, as the window width increases, the error decreases; when the window width is 4,000 earthquakes (blue line), the error is barely 1%. Overall, the relative errors of entropy range between 0.5% and 2% for window widths of > 500 cumulative earthquakes. From this point of view, the choice of *W* must be a reasonable compromise between calculated errors and the visibility of the results. We ultimately chose a window of $W = 3{,}000$ earthquakes (yellow line), for which the relative error of entropy is close to 1% and remains practically constant.

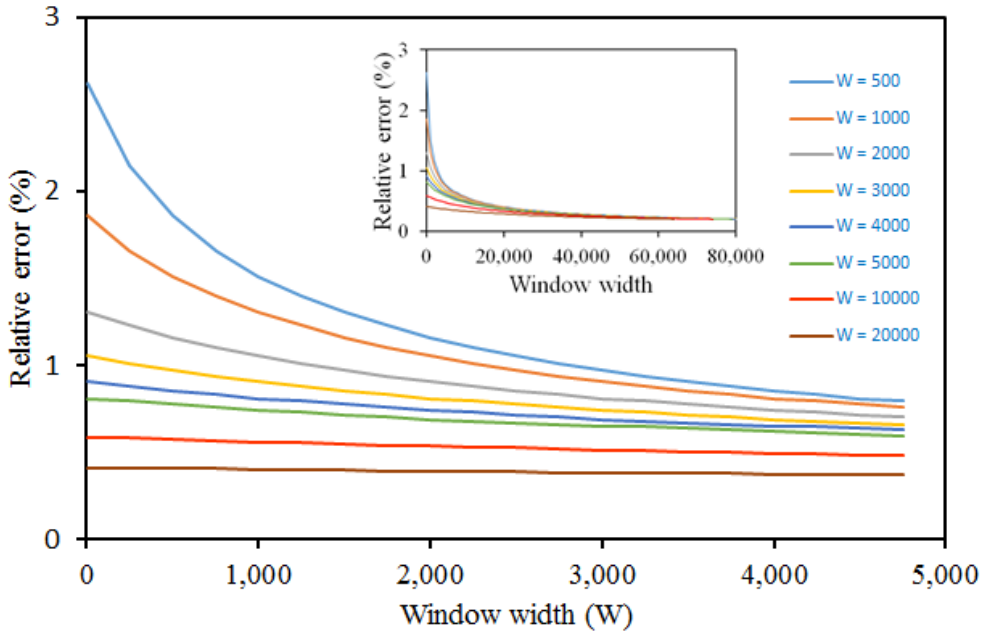

Figure 4. Relative error as a function of the given initial window width. For example, the cyan line corresponds to an initial window width of W = 500, for which the calculated relative error in entropy is 2.7%.

The threshold magnitude and width of the window for the windowing process have been set to $M_0 = 2.2$ and $W = 3{,}000$, respectively; this reduced the size of the catalogue to 84,593 events. Finally, the third step is to get Entropy H. The evolution of entropy with time from the windowing process is shown in Figure 5. Sudden changes in entropy are evident and correspond to the times of the largest earthquakes. Levels of change in the absolute values of entropy increase with increasing earthquake magnitude. The entropy change for the Tocopilla earthquake reached $H = 0.35$, while for the Calama 2010 and 2011 earthquakes, it barely exceeded $H = 0.25$. For the Iquique earthquake and its large foreshock and aftershock, the entropy value reached $H = 0.45$.

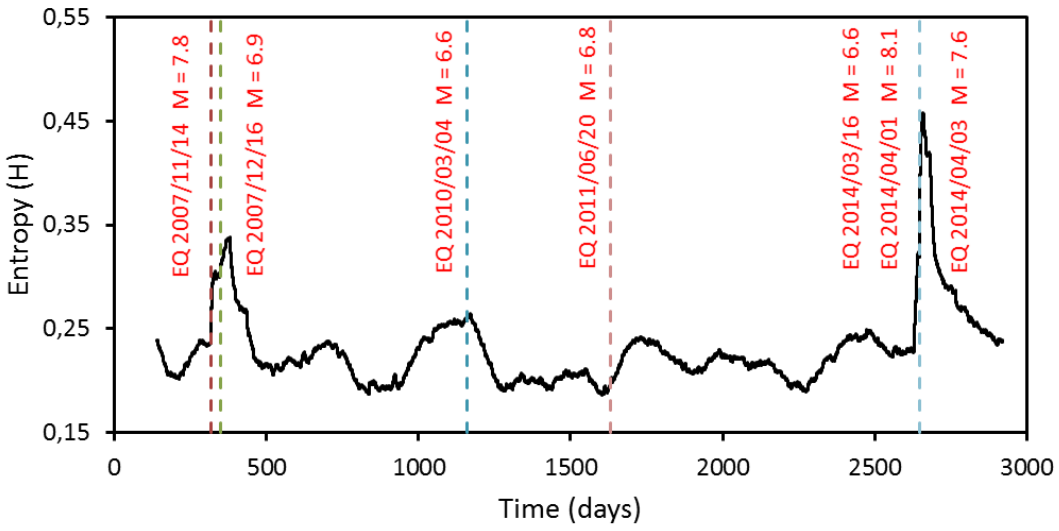

Figure 5. Time series of Shannon entropy, H, with the occurrence times of M_W > 6.5 earthquakes shown by dashed lines (note that the large foreshock, mainshock, and large aftershock of the Iquique earthquake occurred close together in time; as such, only a single dashed line is shown). Sudden changes in entropy are clearly identifiable and coincident with large earthquakes.

Chilean seismicity is not only shallow seismicity; in fact, deep abundant earthquakes occur as correspond to a subduction region; then, we also investigated entropy variation as a function of earthquake type, as defined by depth (Figures 1c and 6), as follows. Zone A: intraplate earthquakes characterised by shallow depth (0–80 km) and a tectonic origin.
235 Zone B: interplate earthquakes characterised by intermediate depth (80–160 km) and related to the contact between the two plates. Zone C: slab earthquakes that occur at large depths (> 160 km) in the slab of the underlying plate.

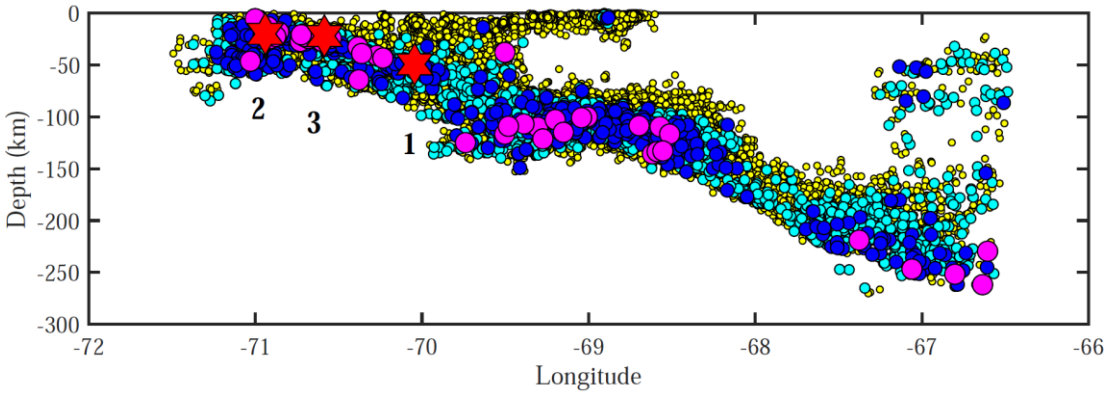

Figure 6. Earthquake depth versus longitude for earthquakes with magnitudes of > 2.0. Circle colours denote event magnitudes: yellow = 2.0–3.9, cyan = 4.0–4.9, blue = 5.0–5.9, and magenta = 6.0–6.9. Red stars denote earthquakes with magnitudes of > 7.0, including the (1) 2007 M_W 7.8 Tocopilla earthquake, (2) 2014 M_W 8.1 Iquique earthquake, and (3) 2014 M_W 7.6 aftershock of the Iquique earthquake.

The analysis of threshold magnitudes for zones A, B, and C, as well as the calculation of window W were as described above for the previous calculation of H (see Figure 7 for epicentral maps of the three zones and the computation of M_0 in each). Figure 8 shows the time series of entropy for each of the three zones. In zone A, sudden changes in entropy were coincident with the Tocopilla and Iquique earthquakes. Zones B and C show low-amplitude sawtooth fluctuations in entropy (maximum ΔH of ≤ 0.09 vs. $\Delta H \approx 0.5$ in zone A). The entropy variations in zones B and C are negligible compared with those in zone A.

In zone B (Figure 8), the 2010 and 2011 Calama earthquakes (M_W 6.6 and M_W 6.8 events on days 1,158 and 1,631, corresponding to April 4, 2010 and June 20, 2011, respectively) are clearly identifiable by increases in entropy. Other peaks before and after these earthquakes are coincident with either smaller earthquakes or clusters of smaller earthquakes (M_W 5.5–6.5), including a M_W 6.5 event on March 24, 2008 (day 448); a group of earthquakes between December 4, 2008 and March 27, 2009 (days 703–816, magnitudes of 5.8–6.0), a M_W 5.9 earthquake on August 8, 2012 (day 2,107); a cluster of earthquakes between July 10, 2013 and January 7, 2014 (days 2,382–2,563, magnitudes of 5.9–6.2); and, two earthquakes on March 31 and August 23, 2014, both with magnitudes of 6.2 (days 2,646 and 2,791, respectively).

A visual analysis of figure 8 seems to indicate that there is a periodic behaviour in the temporal signal of entropy; Although this behaviour seems evident in zone B, it is not so evident in zones A and C. Zone A is associated with a stress loading rate usually not uniform in time because, as is well known, the strength of the crust is not constant; Then, change in entropy is only appreciated when the two great earthquakes occurred. On the other hand, zone C, where the most complex physical phenomena occur due to the rheological state of the materials, seems to exhibit a half-period in the entropic signal, but this must be confirmed in further studies with up-to-date data. The apparent periodicity in zone B suggests carrying out a Fourier analysis of the entropic signal. The entropic signal is not uniformly sampled in the time domain; for this reason, it was averaged to the tenth part of the day and, subsequently, an interpolation was made for points with no sample. Thus, the resulting entropic signal was uniformly sampled and a fast Fourier transform was feasible.

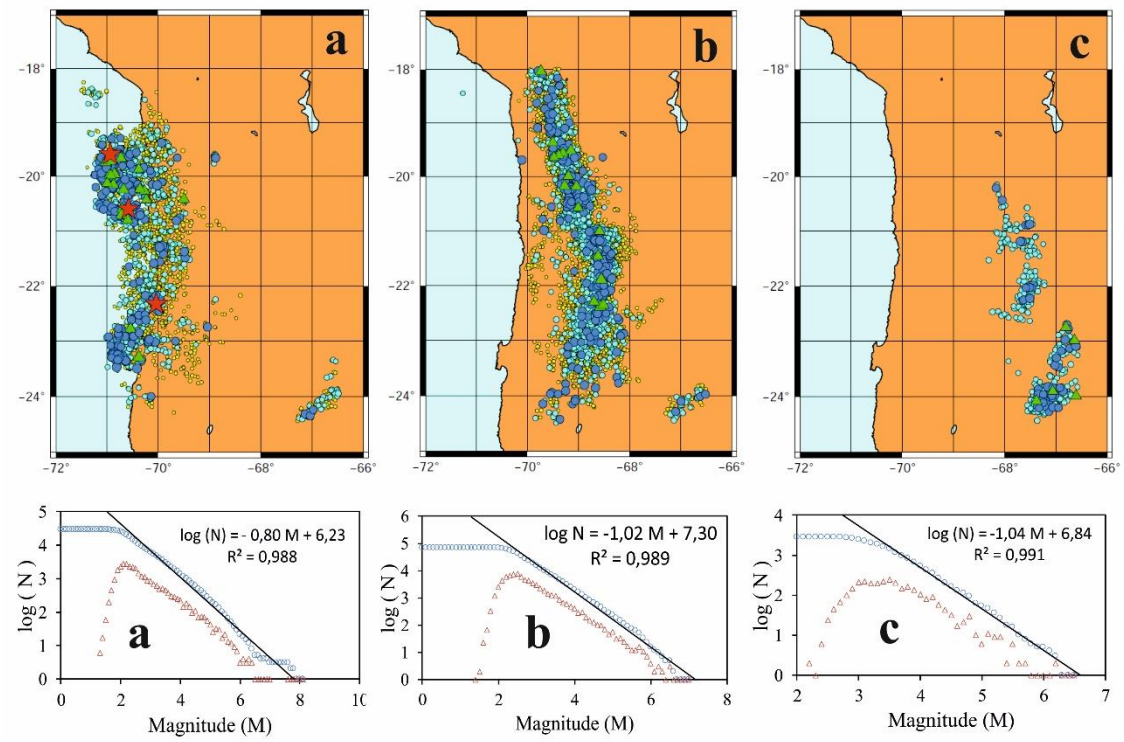

Figure 7. Epicentrally represented earthquake activity and non-cumulative and cumulative Gutenberg–Richter relationships in zones A–C for earthquakes with magnitudes of > 3.0. (a) Zone A (0–80 km), (b), zone C (80–160 km), and (c) zone C (>160 km). Symbol colours denote earthquake magnitude: yellow circles = 3.0–3.9, cyan circles = 4.0–4.9, blue circles = 5.0–5.9, green triangles = 6.0–6.9, and red stars = > 7.0. Based on the maximum curvature (MAXC) technique (Wiemer and Wyss, 2000), M_0= 2.2 in zones *A* and B, and 3.2 in zone C.

270

The Fourier transform of the entropic signal (Figure 9) revealed that the peaks of the predominant amplitude have frequencies of 0.00048 and $0.00119\ days^{-1}$, corresponding to periods of ~2,100 and 840 days, respectively. The 840-day period approximately reproduces the sequence of M > 5.5 earthquakes. For instance, 840 days
275 after the Tocopilla earthquake (November 14, 2007) was March 3, 2010, which is 1 day before the 2010 Calama 2010. However, given the relatively short period covered by the data (8 years), this Fourier analysis is necessarily preliminary. Further studies with observation periods from 2015 until the present are needed to confirm these results.

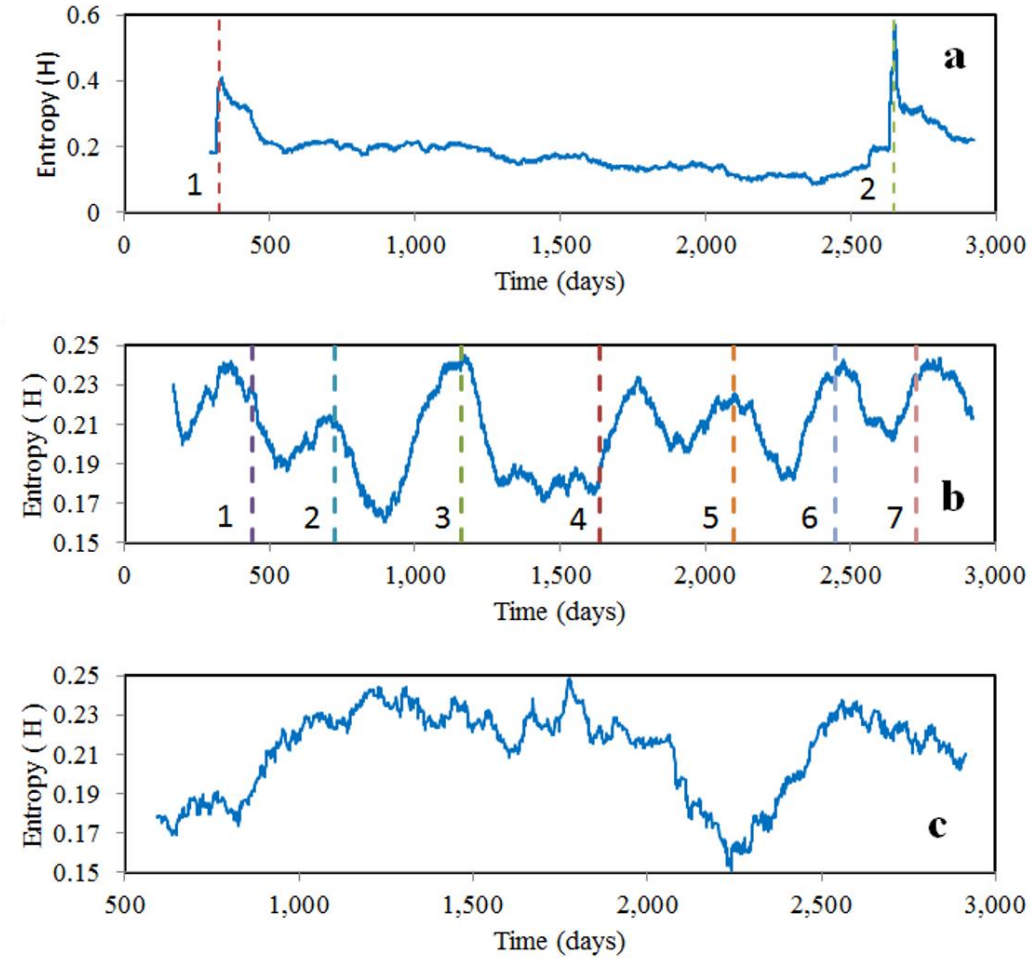

Figure 8. Time series of Shannon entropy, H, within different depth intervals. (a) Zone A (earthquakes with depths of 0–80 km), (b) zone B (80–160 km), and (c) zone C (> 160 km). The relative change in entropy in zone A is ~0.5 units compared with 0.09 units in zones B and C. Lines 1 and 2 in (a) correspond to the 2007 M_W 7.8 Tocopilla earthquake and M_W 8.1 Iquique earthquake, respectively; lines 1 to 7 in (b) correspond to the M_W 6.5 March 2008 earthquake, clusters of earthquakes with magnitudes ranging from 5.8 to 6.0 from December 2008 to March 2009, the 2010 M_W 6.6 Calama earthquake, the 2011 M_W 6.8 Calama earthquake, the 2012 M_W 5.9 earthquake, clusters of earthquakes with magnitudes ranging from 5.9 to 6.2 from July 2013 to January 201, and the two 2014 M_W 6.2 earthquakes.

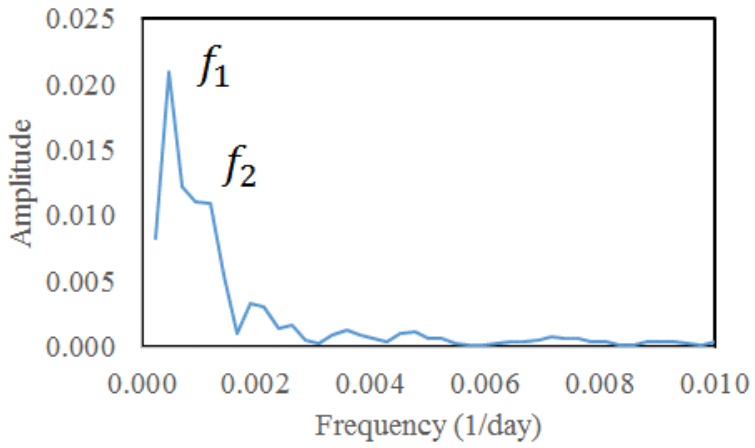

Figure 9. Spectrum for the entropic signal of zone B (80–160 km). The two peak amplitudes have frequencies of $f_1 = 0.00048\ \text{day}^{-1}$ and $f_2 = 0.00119\ \text{days}^{-1}$, corresponding to periods of ~2,100 and 840 days, respectively.

5 Discussion and conclusions

It is widely accepted that the seismic cycle (or "seismic system") comprises six main stages (Figure 10) (Derode et al., 2021; Akopian and Kocharian, 2014). The stages are: (1) Over decades or years, small and medium asperities break continuously, resulting in a uniform rate of seismicity. (2) Asperities become locked, resulting in stress accumulation and decreasing seismic activity. (3) Weeks or days before a mainshock, important asperities progressively break along some sections (i.e., the foreshock stage). (4) Over a scale of hours, accumulated stresses overcome friction and blockages in the main asperities, causing the largest magnitude earthquake of the cycle. (5) Stress relaxation occurs after the mainshock and is characterised by numerous aftershocks of smaller magnitude over several weeks or months; this ceases when new asperities become locked. (6) Finally, the system returns to the initial, long-term, state.

In this paper, we have visualized that this mechanical description of the seismic cycle has an energetic analogy in terms of statistical physics and the Second Law of Thermodynamics. As argued in detail by De Santis *et al.* (2019), an earthquake can be considered as a phase transition, where continuous reorganization of stresses and forces reflects an evolution from equilibrium to non-equilibrium states. Therefore, entropy, which measures the number of accessible states for the present conditions of the systems, can be used as an indicator of the evolution of the system (e.g., (Telesca *et al.*, 2004, Vogel *et al.*, 2020). Stages 1–3 correspond to increasing stresses and the accumulation of seismic energy. During this inter-seismic period, the magnitudes of earthquakes are relatively uniform (or 'ordered') and entropy is relatively low. When a large earthquake occurs (stage 4), the rupture process triggers earthquakes with magnitudes of all sizes in a chaotic way, evolving to new conditions reaching a wider range of microstates in a disordered way, and the entropy increases. Finally, during the post-seismic state (stages 5 and 6), the system progressively recovers conditions similar to the initial ones.

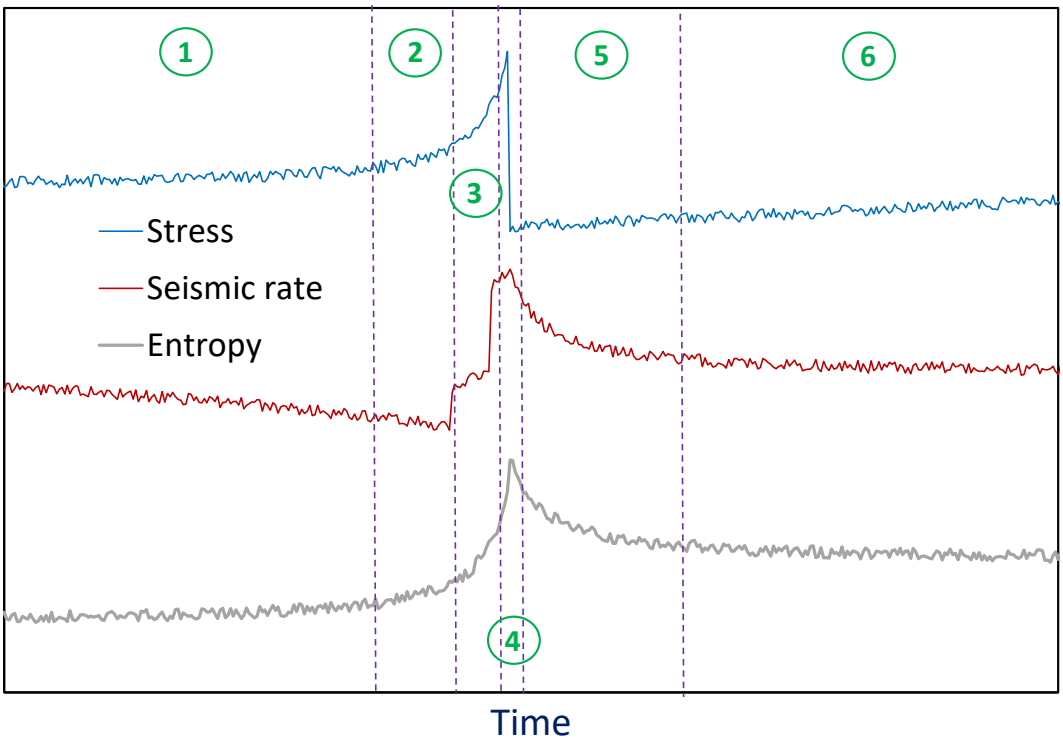

Figure 10. Seismic cycle from a mechanical perspective (i.e., stresses and seismic rate, which are shown in blue and red, respectively) and from a thermodynamic perspective (i.e., entropy, H, which is shown in grey). (1) Stage 1, the interseismic period, is characterised by approximately constant stress, seismic rate, and H. (2) Stage 2, the accumulation period, is characterised by modest increases in stress and H, but a modest decrease in seismic rate. (3) Stage 3, the foreshocks period, is characterised by increasing stress, seismic rate, and H. (4) Stage 4, the coseismic period, is characterised by an abrupt decrease in stress, but increases in the seismic rate and H. (5) Stage 5, the postseismic and aftershock period, is characterised by decreasing stress (i.e., relaxation), seismic rate, and H (towards the initial value). (6) Stage 6, during which the seismic cycle starts again.

Increasing entropy, *H*, from a thermodynamic perspective, is associated with an irreversible transition from one state to another on both small (Scholz, 1968) and large (e.g., Parsons *et al.*, 2008) scales. Using a high-quality catalogue of seismicity in northern Chile, made possible owing to the IPOC network, we confirmed a strong temporal correlation between entropy and the occurrence of earthquakes. Using the entropy value, we could identify all earthquakes with magnitudes of > 6.5 in the catalogue. (i.e., seven events from 2007 to 2014, with magnitudes ranging from 6.6 to 8.1)

However, it is important to note that changes in entropy are detected by analysing the entire catalogue; that is, to detect a change in entropy associated with any event, data from both before and after the event must be analysed. At present, this limits the use of this method for seismic prediction. Further study is needed to determine a robust approach for predicting how a time series will continue without prior knowledge; that is, to determine threshold entropy values and trends that can be used to predict a significant event in the immediate future. To achieve this, an absolute scale of entropy will be necessary.

Earthquakes in zone A (0–80 km depth) tend to be tectonic in origin and have higher magnitudes than those in zones B and C (i.e., intermediate and deep earthquakes); as such, they are of most concern from a risk management perspective. Our results show that the entropy changes associated with such events are much stronger when only data from this depth interval is considered; variations are of the order of one hundredth in zones B and C, but several tenths in zone A.

Data availability. The data are public and available at https://www.ipoc-network.org/data/ and in *Sippl et al. (2018)* available at http://doi.org/10.5880/GFZ.4.1.2018.001.

Author contributions. All authors contributed equally to the design of the methodology, discussion, analysis and revisions of the manuscript.

Competing interests. The authors declare no competing interests.

Acknowledgements. We would like to express our gratitude to the Integrated Plate Boundary Observatory Chile (IPOC) for collecting and sharing the data used in this work.

Financial support. This work was funded partiually by the Spanish State Research Agency (SRA) under the grant PID2021-124701NB-C21 y C22., partially by the FEDER/UAL Project UAL2020-RNM-B1980 and also partially by the research group RNM104 of the Junta de Andalucía. The University of Almeria funding for open access charge if applicable. EEV was supported by Fondecyt (grant number 1230055) and ANID through the Center for Development of Nanoscience and Nanotechnology (CEDENNA; grant number AFB220001).

References

Akopian, S. T.: Open dissipative seismic systems and ensembles of strong earthquakes: Energy balance and entropy funnels, Geophys. J. Int. 201, 1618–1641, doi.org/10.1093/gji/ggv096, 2015.

Akopian, S. T. and Kocharian, A. N.: Critical behaviour of seismic systems and dynamics in ensemble of strong earthquakes, Geophys. J. Int. 196, 580–599, doi: 10.1093/gji/ggt398, 2014.

Amorèse, D.: Applying a change-point detection method on frequency-magnitude distributions, B. Seismol. Soc. Am., 97, 1742–1749, doi:10.1785/0120060181. 2007.

Ben-Naim, A.: Entropy, Shannon's measure of information and Boltzmann's H- theorem, Entropy, 19-48, doi: 10.3390/e19020048, 2017.

Ben-Naim, A.: Entropy and time, Entropy, 22(4), 430, doi: 10.3390/e22040430, 2020.

Cao, A. M. and Gao, S. S.: Temporal variations of seismic b-values beneath northeastern japan island arc, Geophys. Res. Lett. 29(9), 1334; doi:10.1029/2001GL013775, 2002.

Cesca, S., Grigoli, F., Heimann, S., Dahm, T., Kriegerowski, M., Sobiesiak, M., Tassara, C. and Olcay, M.: The Mw 8.1 2014 Iquique, Chile, seismic sequence: a tale of foreshocks and aftershocks, Geophys. J. Int., 204, 1766–1780, doi: 10.1093/gji/ggv544, 2016.

Clausius, R.: Mechanical theory of heat, London, UK, John van Voorst, 1865.

D'Alessandro, A., Luzio, D., D'Anna, G. and Mangano, G.: Seismic Network Evaluation through Simulation: An Application to the Italian National Seismic Network, B. Seismol. Soc. Am. 101, 1213–1232, doi: 10.1785/0120100066, 2011.

De Santis, A., Cianchini, G., Favali, P., Beranzoli, L. and Boschi, E.: The Gutenberg-Richter Law and Entropy of Earthquakes: Two Case Studies in Central Italy, B. Seism. Soc. Am., 101, 1386–1395, doi: 10.1785/0120090390, 2011.

De Santis, A., Abbattista, C., Alfonsi, L., Amoruso, L., Campuzano, S., Carbone, M., Cesaroni, C., Cianchini, G., De Franceschi, G., De Santis, A., Di Giovambattista, R., Marchetti, D., Martino, L., Perrone, L., Piscini, A., Rainone, M., Soldani, M., Spogli, L. and Santoro, F.: Geosystemics View of Earthquakes, Entropy, 21, 412-442, doi.org/10.3390/e21040412, 2019.

Delouis, B., Pardo, M., Legrand, D. and Monfret, T.: The MW 7.7 Tocopilla Earthquake of 14 November 2007 at the Southern Edge of the Northern Chile Seismic Gap: Rupture in the Deep Part of the Coupled Plate Interface, B. Seismol. Soc. Am. 99(1), 87–94, doi:10.1785/0120080192, 2009.

Derode, B., Madariaga, R. and Campos, J.: Seismic rate variations prior to the 2010 Maule, Chile MW 8.8 giant megathrust earthquake, Sci. Rep-UK, 11, 2705, doi.org/10.1038/s41598-021-82152-0, 2021.

Feng, L. and Luo, G.: The relationship between seismic frequency and magnitude as based on the Maximum Entropy Principle, Soft Comput., 13, 979–83, doi: 10.10 07/s0 050 0-0 08-0340-x, 2009.

Gutenberg, B. and Richter, C. F.: Frequency of earthquakes in California, B. Seismol. Soc. Am., 34, 185-188, 1944.

Khordad, R., Rastegar Sedehi, H.R. and Sharifzadeh, M.: Susceptibility, entropy and specific heat of quantum rings in monolayer graphene: comparison between different entropy formalisms, J. Comput. Electron., 21, 422–430, doi.org/10.1007/s10825-022-01857-1, 2022.

Majewski, E.: Thermodynamics of chaos and fractals applied: evolution of the earth and phase transformations, in: Earthquake thermodynamics and phase transformations in the Earth's interior, edited by Teisseyre, R. and Majewski, E., Academic Press, 25–78, ISBN 9780080530659, 2001.

Majewski, E. and Teisseyre, R.: Earthquake thermodynamics, Tectonophysics, 277, 219–233, doi: 10.1016/S0 040-1951(97)0 0 088-7, 1997.

Michas, G., Vallianatos, F. and Sammonds, P.: Non-extensivity and long-range correlations in the earthquake activity at the west Corinth rift (Greece), Nonlinear Proc. Geoph., 20, 713–724, dx.doi.org/10.5194/npg-20-713-2013, 2013.

Nikulov, A.: The Law of Entropy Increase and the Meissner Effect, Entropy, 24, 83, doi.org/10.3390/e24010083, 2022.

Ogata, Y. and Katsura, K.: Analysis of temporal and spatial heterogeneity of magnitude frequency distribution inferred from earthquake catalogues, Geophys. J. Int.. 3(113), 727–738, doi: 10.1111/j.1365-246X.1993.tb04663.x, 1993.

Papadakis, G., Vallianatos, F. and Sammonds, P.: A nonextensive statistical physics analysis of the 1995 Kobe, Japan earthquake, Pure Appl. Geophys., 172, 1923–1931, dx.doi.org/10.1007/s00024-014-0876-x, 2015.

Parsons, T., Ji, C. and Kirby, E.: Stress changes from the 2008 Wenchuan earthquake and increased hazard in the Sichuan basin, Nature, 454, 509–510, doi: 10.1038/nature07177, 2008.

Pasten, D., Saravia, G., Vogel, E. and Posadas, A.: Information theory and earthquakes: depth propagation seismicity in northern Chile, Chaos Soliton Fract., 165, 2, 112874, doi.org/10.1016/j.chaos.2022.112874, 2022.

Posadas, A. and Sotolongo-Costa, O.: Non-extensive entropy and fragment–asperity interaction model for earthquakes, Commun. Nonlinear Sci., 117, 106906, doi.org/10.1016/j.cnsns.2022.106906, 2023.

Posadas, A., Morales, J., Ibáñez, J. and Posadas-Garzon, A.: Shaking earth: Non-linear seismic processes and the second law of thermodynamics: A case study from Canterbury (New Zealand) earthquakes, Chaos Soliton Fract., 151, 111243, doi.org/10.1016/j.chaos.2021.111243, 2021.

Rastegar Sedehi, H.R., Bazrafshan, A. and Khordad, R.: Thermal properties of quantum rings in monolayer and bilayer graphene, Solid State Commun., 353, 114853. doi.org/10.1016/j.ssc.2022.114853, 2022.

Rundle, J.B., Turcotte, D.L., Shcherbakov, R., Klein, W. and Sammis, C.: Statistical physics approach to understanding the multiscale dynamics of earthquake fault systems, Rev. Geophys., 41, 1019–1049, doi:10.1029/2003RG000135, 2003.

Rydele, P. A. and Sacks, I. S.: Testing the completeness of earthquake catalogs and the hypothesis of self-similarity, Nature, 337, 251–253, doi: 10.1038/337251a0, 1989.

Sarlis, N. V., Skordas, E. S. and Varotsos, P. A.: A remarkable change of the entropy of seismicity in natural time under time reversal before the super-giant M9 Tohoku earthquake on 11 March 2011, Europhys. Lett., 124, 29001–29008, doi: 10.1209/0295-5075/124/29001, 2008.

Shannon, C. E.: The mathematical theory of communication, Bell Syst. Tech. J., 27, 379–423, 1948.

Shannon, C. E., Weaver, W.: The Mathematical Theory of Communication, The Board of Trustees of the University of Illinois, 1949.

Scholz, C. H.: The frequency–magnitude relation of microfracturing in rock and its relation to earthquakes, B. Seismol. Soc. Am., 58, 399–415, doi: 10.1785/BSSA0580010399, 1968.

Sippl, C., Schurr, B., Asch, G. and Kummerow, J.: Seismicity structure of the northern Chile forearc from >100,000 double-difference relocated hypocenters, J. Geophys. Res-SOL. EA., 123, 4063–4087, doi: 10.1002/2017JB015384, 2018.

Sornette D. and Werner M.J.: Statistical physics approaches to seismicity, In: Meyers R.A., editor, Encyclopedia of complexity and systems science, Springer, 7872–7891, doi: 10.1007/978-0-387-30440-3_467, 2009.

Telesca, L., Lapenna, V. and Lovallo, M.: Information entropy analysis of Umbria-Marche region (central Italy), Nat. Hazards Earth Sys. 4, 691–695, doi: 10.5194/nhess-4-691-2004, 2004.

Telesca, L., Thai, A.T., Lovallo, M., Cao, D.T. and Nguyen, L.M.: Shannon Entropy Analysis of Reservoir-Triggered Seismicity at Song Tranh 2 Hydropower Plant, Vietnam, Appl. Sci., 12, 8873, doi.org/10.3390/app12178873, 2022.

Truffet, L.: Shannon Entropy Reinterpreted, Rep. Math. Phys, 81, 3, 303-319, https://doi.org/10.1016/S0034-4877(18)30050-8, 2018.

Tsallis, C.: Possible generalization of Boltzmann-Gibbs statistics, J. Stat. Phys., 52, 479-487, doi.org/10.1007/BF01016429, 1998.

Utsu, T.: A method for determining the value of b in a formula log N = a–bM showing the magnitude-frequency relation for earthquakes, Geophys. Bull. Hokkaido Univ., Jpn, 13, 99–103, 1965.

Utsu T.: Representation and Analysis of the Earthquake Size Distribution: A Historical Review and Some New Approaches, Pure Appl. Geophys., 155, 509–535, doi: 10.1007/s000240050276, 1999.

Vallianatos, F., Michas, G. and Papadakis, G.: A description of seismicity based on non-extensive statistical physics: a review. In: D'Amico S, editor, Earthquakes and their impact on society, Springer Natural Hazards, 1–41. dx.doi.org/10.1007/978-3-319-21753-6, 2015.

Vallianatos, F., Papadakis, G. and Michas, G.: Generalized statistical mechanics approaches to earthquakes and tectonics, Proc. R. Soc. Lond. Ser. A Math. Phys. Eng. Sci., 472, 20160497, http://dx.doi.org/10.1098/rspa.2016.0497, 2016.

Vallianatos, F., Michas, G. and Papadakis, G.: Nonextensive statistical seismology: An overview. In: Chelidze T, Vallianatos F, Telesca L, editors, Complexity of seismic time series, Complexity of seismic time series: Measurement and application, Elsevier, 25–59. dx.doi.org/10.1016/B978-0-12-813138-1.00002-X, 2018.

Vargas, C.A., Flores-Márquez, E.L., Ramírez-Rojas, A. and Telesca, L.: Analysis of natural time domain entropy fluctuations of synthetic seismicity generated by a simple stick–slip system with asperities, Physica A, 419, 23-28, doi.org/10.1016/j.physa.2014.10.037, 2015.

Varotsos, P. A., Sarlis, N. V., and Skordas, E. S.: Scale-specific order parameter fluctuations of seismicity in natural time before mainshocks, Europhys. Lett., 96, 59002, doi 10.1209/0295-5075/96/59002, 2011.

Varotsos, P.A., Sarlis, N.V. and Skordas, E.S.: Order Parameter and Entropy of Seismicity in Natural Time before Major Earthquakes: Recent Results, Geosciences, 12, 225, doi.org/10.3390/geosciences12060225, 2022.

Vogel, E.E., Brevis, F.G., Pastén, D., Muñoz, V., Miranda, R.A. and Chian, A.: Measuring the seismic risk along the Nazca-South American subduction front: Shannon entropy and mutability, Nat. Hazards Earth Sys., 20, 2943–2960, doi.org/10.5194/nhess-20-2943, 2020.

Wiemer, S. and Wyss, M.: Minimum magnitude of complete reporting in earthquake catalogs: examples from Alaska, the Western United States, and Japan, B. Seismol. Soc. Am., 90, 859–869, doi: 10.1785/0119990114, 2000.

Zúñiga, F. and Wyss, M.: Inadvertent changes in magnitude reported in earthquake catalogs: Their evaluation through b-value estimates, B. Seismol. Soc. Am., 85, 1858–1866, doi:10.1785/BSSA0850061858, 1995.

Zupanovic, P. and Domagoj, K.: Relation between Boltzmann and Gibbs entropy and example with multinomial distribution, J. Phys. Commun., 2, 045002, doi: 10.1088/2399-6528/aab7e1, 2018.